

Magnetic Inclination Evolution of Accreting Neutron Stars in Intermediate/Low-Mass X-ray Binaries

HAO-RAN YANG ^{1,2} AND XIANG-DONG LI ^{1,2}

¹*School of Astronomy and Space Science, Nanjing University, Nanjing 210046, China; lixd@nju.edu.cn*

²*Key Laboratory of Modern Astronomy and Astrophysics (Nanjing University), Ministry of Education, Nanjing 210023, China*

ABSTRACT

The magnetic inclination angle χ , namely the angle between the spin and magnetic axes of a neutron star (NS), plays a vital role in its observational characteristics. However, there are few systematic investigations on its long-term evolution, especially for accreting NSs in binary systems. Applying the model of [Biryukov & Abolmasov \(2021\)](#) and the binary evolution code *MESA*, we simultaneously simulate the evolution of the accretion rate, spin period, magnetic field, and magnetic inclination angle of accreting NSs in intermediate/low X-ray binaries (I/LMXBs). We show that the evolution of χ depends not only on the initial parameters of the binary systems, but also on the mass transfer history and the efficiency of pulsar loss. Based on the calculated results we present the characteristic distribution of χ for various types of systems including ultracompact X-ray binaries, binary millisecond pulsars, and ultraluminous X-ray sources, and discuss their possible observational implications.

Keywords: accretion, accretion disks - stars: neutron - X-rays: binaries

1. INTRODUCTION

Neutron stars (NSs) in X-ray binaries accrete both mass and angular momentum from their companion stars. If the NSs are magnetized, the interaction between the magnetic field and the accreting material determines the structure of the magnetosphere and the radiation characteristics. The nature of the interaction depends on whether the NSs are wind-fed or disk-fed, usually corresponding to NSs in high-mass X-ray binaries (HMXBs) and intermediate/low X-ray binaries (I/LMXBs), respectively ([Bhattacharya & van den Heuvel 1991](#)). It is interesting to notice that the torque exerted by the accreting material can simultaneously affect the evolution of the spin period P_s of the NSs ([Ghosh & Lamb 1979](#); [Wang 1987](#)), the spin inclination angle α , and the magnetic inclination angle χ ([Wang & Welter 1981](#); [Leahy 1990](#); [Bulik et al. 2003](#); [Annala & Poutanen 2010](#)). Here α and χ are the angle between the spin axis of the NS and the axis of the orbital plane and the angle between the spin and magnetic axes of the NS, respectively. In the following we adopt a dipolar configuration for the NS magnetic field.

The magnetic inclination angle plays a crucial role in the characteristics of the pulsed radiation from accreting X-ray pulsars and from non-accreting radio pulsars in binaries. The latter are generally related to binary millisecond pulsars (BMSPs), which are thought to evolve from I/LMXBs. Although there are attempts trying to compare theory with observation, definite conclusions are not ready to draw, because reliable data of χ are still limited ([Lyne & Manchester 1988](#);

[Rankin 1990](#); [Young et al. 2010](#); [Venter et al. 2009](#); [Johnson et al. 2014](#); [Benli et al. 2021](#)). Meanwhile, the evolution of the magnetic inclination angles is dependent on the evolution of the accretion rate and the magnetic field of the NS, and the magnetic field-disk interaction, which are currently not well understood.

[Biryukov & Abolmasov \(2021, hereafter BA21\)](#) recently developed a model to trace the NS's magnetic inclination angle evolution for both disk-fed and wind-fed NSs. They showed that the accretion torque can affect the magnetic inclination angle evolution when both α and χ significantly deviate from zero. As the spin axis of the NS is being aligned with the spin-up torque, the magnetic axis becomes misaligned with the spin axis, which is favorable for detection of pulsed radiation from BMSPs. This work focuses on the magnetic inclination angle evolution for disk-fed NSs in I/LMXBs based on the BA21 model. Here we include some critical factors that were not considered by BA21. The most important one is that BA21 used fixed accretion rates in their calculations for convenience, without considering the influence of binary evolution on the change of accretion rates. So their calculations are limited within $10^5 - 10^7$ yr evolution. In realistic situation, the accretion history is much more complicated, depending on the initial conditions of both the NSs and the donors, the mass and angular momentum transfer between the components, and the accretion disk physics (see below). The mass transfer lifetimes in I/LMXBs vary from $\sim 10^8$ yr to 10^{10} yr, so the final magnetic inclination

angles could significantly deviate from those in short-time evolution.

The rest of the paper is organized as follows. In Section 2, we review and slightly modify the BA21 model, and then simulate a grid of I/LMXBs with different initial parameters using the binary evolution code *MESA* (Paxton et al. 2011, 2013, 2015, 2018, 2019). We select five representative systems, corresponding to ultracompac X-ray binaries (UCXBs), traditional LMXBs, IMXBs, and ultraluminous X-ray binaries (ULXs), and calculate their evolution. The results are presented in Section 3. In Section 4, we discuss the possible effects for the adopted parameters and make predictions for future observational test. Finally, the conclusions are given in Section 5.

2. METHOD

2.1. The evolution of an accreting neutron star

In the BA21 approach, the evolution of an accreting NS can be described by a set of differential equations:

$$I\dot{\Omega} = n_1 \cos \alpha + n_2 + n_3(1 + \sin^2 \chi) - \dot{I}\Omega, \quad (1)$$

$$I\Omega\dot{\alpha} = -n_1 \sin \alpha, \quad (2)$$

$$I\Omega\dot{\chi} = \eta A(\eta, \alpha, \chi) n_1 \sin^2 \alpha \cos \alpha \sin \chi \cos \chi + n_3 \sin \chi \cos \chi, \quad (3)$$

where I and Ω are the moment of inertia and angular velocity of the NS, n_1 , n_2 and n_3 represent the averaged torques acting on the NS caused by accretion, magnetic braking due to magnetic field-disk interaction, and pulsar's radiation loss, respectively. The coefficient $0 < \eta \leq 1$ is a constant to describe the accretion torque modulation within the spin period, which is set to unity in accordance with BA21, and $A(\eta, \alpha, \chi)$ is a normalization function,

$$A(\eta, \alpha, \chi) = \left[1 - \frac{\eta}{2} (\sin^2 \chi \sin^2 \alpha + 2 \cos^2 \chi \cos^2 \alpha) \right]^{-1}. \quad (4)$$

The torques acting on the NS can be written as

$$n_1 = \dot{M}_{\text{acc}} (GM_* r_{\text{in}})^{1/2}, \text{ if } r_{\text{in}} < r_{\text{co}}; \quad (5)$$

$$n_2 = -\frac{\mu^2}{3r_{\text{co}}^3}, \text{ if } r_{\text{in}} < r_{\text{lc}}; \quad (6)$$

$$n_3 = -\frac{\mu^2}{r_{\text{lc}}^3}. \quad (7)$$

Here G is the gravitational constant, M_* , μ and \dot{M}_{acc} are the mass, magnetic moment, and mass accretion rate of the NS, respectively. We assume that the accretion rate is the mass transfer rate \dot{M} limited by the Eddington limit accretion rate, that is

$$\dot{M}_{\text{acc}} = \min(\dot{M}, \dot{M}_{\text{Edd}}), \quad (8)$$

where

$$\dot{M}_{\text{Edd}} = 1.43 \times 10^{18} M_{*,\odot} \text{g s}^{-1}, \quad (9)$$

Table 1. Parameters of the selected models in this paper. $M_{2,i}$ and $P_{\text{orb},i}$ represent the initial donor mass and orbital period, respectively. The initial mass of NS is set to $1.4M_{\odot}$ for all models.

Model	A	B	C	D	E
$M_{2,i} (M_{\odot})$	1	1	3.4	3	5
$P_{\text{orb},i} (\text{d})$	1	10	1.58	100	1

and $M_{*,\odot} = M_*/M_{\odot}$.

In Eqs.(5)-(7), r_{in} , r_{co} and r_{lc} are the inner disk radius (or the magnetospheric radius), corotation radius, and light cylinder radius, respectively,

$$r_{\text{in}} = \xi \left(\frac{\mu^4}{2GM_* \dot{M}^2} \right)^{1/7} \simeq 7.5 \times 10^7 \mu_{30}^{4/7} M_{*,\odot}^{-1/7} (\dot{M}/\dot{M}_{\text{Edd},\odot})^{-2/7} \text{cm} \quad (10)$$

$$r_{\text{co}} = \left(\frac{GM_*}{\Omega^2} \right)^{1/3} \simeq 1.5 \times 10^8 M_{*,\odot}^{1/3} P_{s,1}^{2/3} \text{cm}, \quad (11)$$

$$r_{\text{lc}} = \frac{c}{\Omega} \simeq 4.8 \times 10^9 P_{s,1} \text{cm}. \quad (12)$$

where $\xi \sim 0.5$ is a correction coefficient depending on the detailed structure of the disk (Ghosh & Lamb 1979; Long et al. 2005; Bessolaz et al. 2008), $\mu_{30,0} = \mu/10^{30} \text{G cm}^3$ and $P_{s,1} = P/1\text{s}$ are the normalized magnetic dipole moment and spin period of the NS, respectively. Equation (10) is derived by assuming that the total matter (ram and gas) pressure is balanced by the total magnetic pressure at r_{in} , which is generally consistent with axisymmetric and global 3D MHD simulations (Kulkarni & Romanova 2013). Since there is no specific restriction on the geometry of the stellar magnetic field in this formula (Romanova & Owocki 2015), it has also been adopted in more complicated situations, including those that are non-stationary and with tilted magnetic and rotational axes (e.g., Romanova et al. 2021).

We also consider the accretion-induced field decay in the following form (Shibazaki et al. 1989; Zhang & Kojima 2006; Liu & Li 2019),

$$\mu = \mu_{\text{min}} + \mu_0 \left(1 + \frac{\Delta M_*}{10^{-5} M_{\odot}} \right)^{-1}. \quad (13)$$

where μ_0 , μ_{min} , and ΔM_* are the initial magnetic moment, the bottom magnetic moment, and the amount of matter accreted by the NS, respectively. We set $\mu_{\text{min}} = 10^{26} \text{G cm}^3$, to be comparable with the weakest magnetic fields of pulsars.

2.2. Evolution of I/LMXBs

We follow the long-term binary evolution using the stellar evolution code *MESA* (version number 15140). The NS is taken to be a point mass whose initial mass is set to $1.4M_{\odot}$, and the metallicity of the donor is $Z = 0.02$. We evolved a

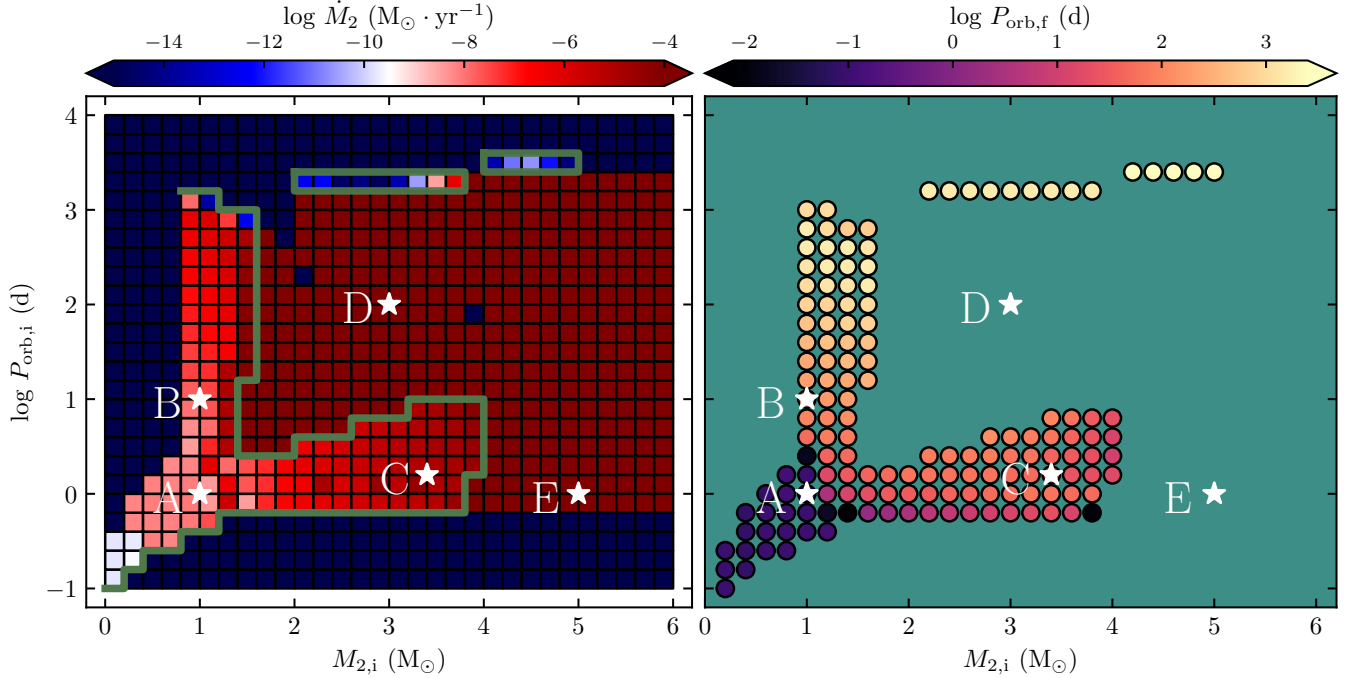


Figure 1. Distributions of I/LMXBs in the $M_{2,i} - P_{orb,i}$ plane, colored by the magnitude of the maximum mass transfer rate \dot{M}_2 (left panel) and the final orbital period $P_{orb,f}$ (right panel). The green lines in the left panel confine the parameter space that have stable mass transfer. The white stars in both panels are the selected systems used in our calculations, and their parameters are listed in Table 1.

large number of incipient NS I/LMXBs with the donor mass varying from $0.2M_\odot$ to $6M_\odot$ by steps of $0.2M_\odot$, and the orbital period (in units of days) logarithmically ranging from -1 to 3 by steps of 0.2 . The [Ritter \(1988\)](#) scheme was used to compute the mass transfer rates via Roche-lobe overflow (RLOF). Besides, we considered magnetic braking and gravitational wave radiation for angular momentum loss from the binary.

Figure 1 illustrates the distribution of I/LMXBs in the initial donor mass-orbital period plane. In the left panel, the color of each element represents the maximum mass transfer rate \dot{M}_2 , the magnitude of which is indicated by the color bar on the top of the figure. If the maximum mass transfer rate is larger than $10^{-4}M_\odot\text{yr}^{-1}$, we regard the mass transfer to be dynamically unstable, followed by common envelope (CE) evolution; if the maximum mass transfer rate is smaller than $10^{-15}M_\odot\text{yr}^{-1}$ we regard that no mass transfer via RLOF has occurred. Systems in between are confined by the green lines, and identified to experience stable mass transfer. They are plotted in the right panel with the color denoting the magnitude of their final orbital periods $P_{orb,f}$, also indicated by the top color bar. The white stars labeled A-E in both panels are representative systems used in our following calculations whose initial parameters are listed in Table 1. The five systems have distinct evolutionary paths, three of which (A, B and C) are located in the parameter space of stable mass

transfer and the other two (i.e. D and E) are outside the parameter space.

Systems A and B are LMXBs with the same initial donor mass ($1M_\odot$) but different initial orbital periods. They will follow different evolutionary paths. In system A, because of its relatively short orbital period (1 d), mass transfer is driven by orbital angular momentum loss caused by magnetic braking and gravitational wave radiation. It starts early and lasts $\sim 10^{10}$ yr, and the donor always remains in main-sequence. The binary will finally evolve to be an UCXB (and probably a black widow/redback binary). The initial orbital period of system B is 10 d, longer than the bifurcation period which separates the converging binary systems from the diverging binary systems ([Pylyser & Savonije 1988, 1989](#)). Its mass transfer is driven by nuclear evolution of the donor, which will finally evolve to be a Helium white dwarf (He WD). The duration ($\sim 10^8$ yr) of the mass transfer is significantly shorter than in System A. After the mass transfer ceases, the final evolutionary outcome is a BMSP.

Systems C, D and E start evolution as IMXBs and can appear as ULXs. Among them, system C experiences thermal-timescale mass transfer at first, and then evolves to be an LMXB after the mass ratio reverses. The donor eventually becomes a hybrid Carbon-Oxygen white dwarf (CO WD). The remaining two systems (D and E) are subject to delayed dynamically unstable mass transfer because the initial orbital period is too long (100 d) or the donor is too massive ($5M_\odot$).

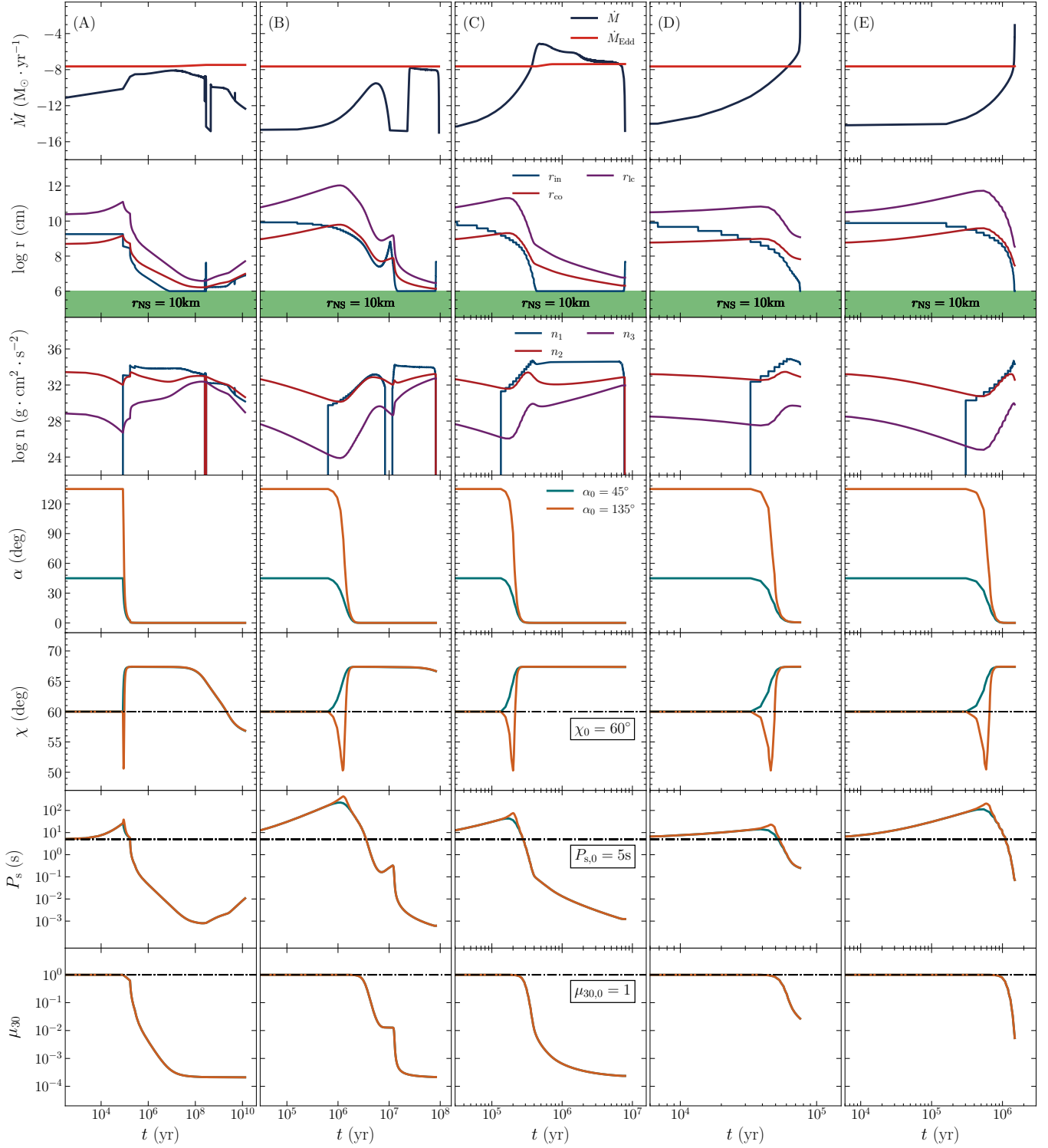


Figure 2. Evolution of different parameters for systems A-E (from left to right). The rows from top to bottom show the change of the mass transfer rates, the three radii (r_{in} , r_{co} and r_{lc}), three torques, the spin inclination angle α , the magnetic inclination angle χ , the spin period P_s , and the magnetic moment μ_{30} with time.

The mass transfer rates rise rapidly to exceed the Eddington limit accretion rate, and they will enter CE evolution, probably leading to merger of both components.

Knowing the mass transfer history, we can follow the evolution of the spin period and the magnetic inclination angle for given initial parameters. It is potentially possible to pre-

dict the distribution of the magnetic inclination angles of the NSs in different evolutionary stages.

3. RESULTS

Figure 2 shows the calculated results (in solid lines) for the five systems. The initial parameters at the beginning of mass transfer are taken to be in accordance with BA21 for the convenience of comparison: the magnetic inclination angle $\chi_0 = 60^\circ$, the spin inclination angle $\alpha_0 = 45^\circ$ and 135° (indicated by the blue and orange lines, respectively), the spin period¹ $P_{s,0} = 5$ s, and the normalized magnetic dipole moment $\mu_{30,0} = \mu_0/10^{30} \text{ G cm}^3 = 1$. The panels from top to bottom in Figure 2 demonstrate the evolution of the mass transfer rate, the three radii (r_{in} , r_{co} and r_{lc}), the three torques (n_1 , n_2 and n_3), the spin inclination angle α , the magnetic inclination angle χ , the spin period P_s , and the magnetic moment μ_{30} , respectively. The five rows from left to right correspond to systems A to E, respectively.

We can easily find that the evolution of χ with different α_0 shows similar tendency except in the beginning phase of the mass transfer, which is related to the first term in Eq (3) ($\propto \sin^2 \alpha \cos \alpha$). Moreover, the evolution of χ is similar for all systems except system A. During the first $10^4 - 10^5$ yr of mass transfer, the mass transfer rates \dot{M} are relatively low and there is no or very little accretion, thus little change occurs in both α and χ . The NS is spun down mainly by the magnetic braking torque n_2 . Then, with the decrease in Ω and increase in \dot{M} , n_2 declines and n_1 increases accordingly. Therefore, α starts evolving toward 0° rapidly (within a few $10^4 - 10^6$ yr). During this period, χ increases to $\sim 68^\circ$ (in the case of $\alpha_0 = 135^\circ$, χ decreases firstly because $\cos \alpha < 0$), and keeps nearly unchanged after $\alpha \rightarrow 0^\circ$. At the same time, the accreting NS is spun up by the accretion torque n_1 . Our calculated evolution of χ in these circumstances is in general concordance with the results in BA21. However, we note that the long-term spin evolution of the NS in systems B-E is different despite of the similarity of the χ evolution. The spin periods P_s in system B and C evolve to milliseconds eventually after the accretion ends due to their relatively long accretion time and low magnetic moments ($\sim \mu_{\text{min}}$). The latter reflects effective accretion-induced field decay occurred in the NS. For the other two systems (D and E), the shorter mass transfer time leads to less decayed magnetic moment and a longer P_s . The mass transfer rates in the late stage exceed the Eddington limit by a few orders of magnitude, so these systems would behave as ULXs.

As for system A, the accretion timescale is so long (up to the Hubble time) that the evolution of χ enters another stage. From Eq. (3) we know that the evolution of χ depends on the accretion torques n_1 and the pulsar loss torque n_3 . After α evolves to zero, the change in χ is completely controlled by n_3 . Although its magnitude is relatively small, as the mass transfer proceeds for sufficiently long time, n_3 drives χ to decrease to $\sim 55^\circ$.

To explore the influence of the magnetic moment, we set the initial parameters to be $\alpha_0 = 45^\circ$, $\chi_0 = 60^\circ$ and $P_0 = 5$ s, and change $\mu_{30,0}$ from 0.01 to 100. This range roughly covers the magnetic field strengths of weakly magnetized NSs to magnetars. Figure 3 shows the evolution of the three radii (r_{in} , r_{co} and r_{lc}) and the magnitude of the three torques (n_1 , n_2 and n_3) with different $\mu_{30,0}$, and Figure 4 shows the corresponding evolution of χ , α , P_s and μ_{30} .

We first examine the evolution of system A, which is demonstrated in the first column in Figures 3 and 4. When $\mu_{30,0} \geq 1$, r_{in} is comparable with r_{co} at the beginning of the mass transfer, and the NS experiences an episode of spin-down. The longest period that the NS can reach increases with $\mu_{30,0}$. After that the NS enters the accretor phase and the accretion torque n_1 begins to work. We note that the stronger $\mu_{30,0}$ is, the earlier the accretor phase starts, and α and χ begin to decrease and increase earlier, respectively. After about 10^6 yr, the mass transfer rate gets higher, accretion causes μ_{30} to decrease significantly, leading to smaller r_{in} and stronger n_1 . The NS starts spinning up rapidly. Accordingly, both r_{co} and r_{lc} become smaller, resulting in more effective spin-down torques (n_2 and n_3) to balance n_1 , which not only set the spin period to be around the equilibrium spin period², but also cause χ to decrease. Because the magnitude of n_3 increases with $\mu_{30,0}$, the larger $\mu_{30,0}$, the smaller the final χ . On the other hand, if the initial magnetic field is relatively weak ($\mu_{30,0} < 1$), the NS directly enters the accretor phase at the beginning of the mass transfer. Smaller magnetic moments lead to less change in χ . Similar tendency can be found in systems B-E, except the case of $\mu_{30,0} = 100$, in which the initial inner disk radius is beyond the light cylinder radius, and the NS enters the radio pulsar phase at the beginning. This causes the magnetic inclination angle χ to decrease for $\sim 10^4 - 10^5$ yr before accretion begins. After that, χ increases and then settles down. If the mass transfer lasts sufficiently long time, χ will finally decreases. The early radio pulsar episode leads to the smallest χ after accretion ends in the five systems.

² After the NS reaches the equilibrium period, r_{in} alternates between $\lesssim r_{\text{co}}$ and $\gtrsim r_{\text{co}}$, and the accretion torque n_1 correspondingly switches between zero and non-zero values according to Eq. (5). In Figure 3 we only show the non-zero values of n_1 for clarity.

¹ Before the mass transfer occurs, the NS is slowed down to a relatively long spin period due to magnetic dipole radiation. We have performed calculations with $P_{s,0}$ ranging from 10 ms to 10 s, and found that the results are insensitive to the value of $P_{s,0}$.

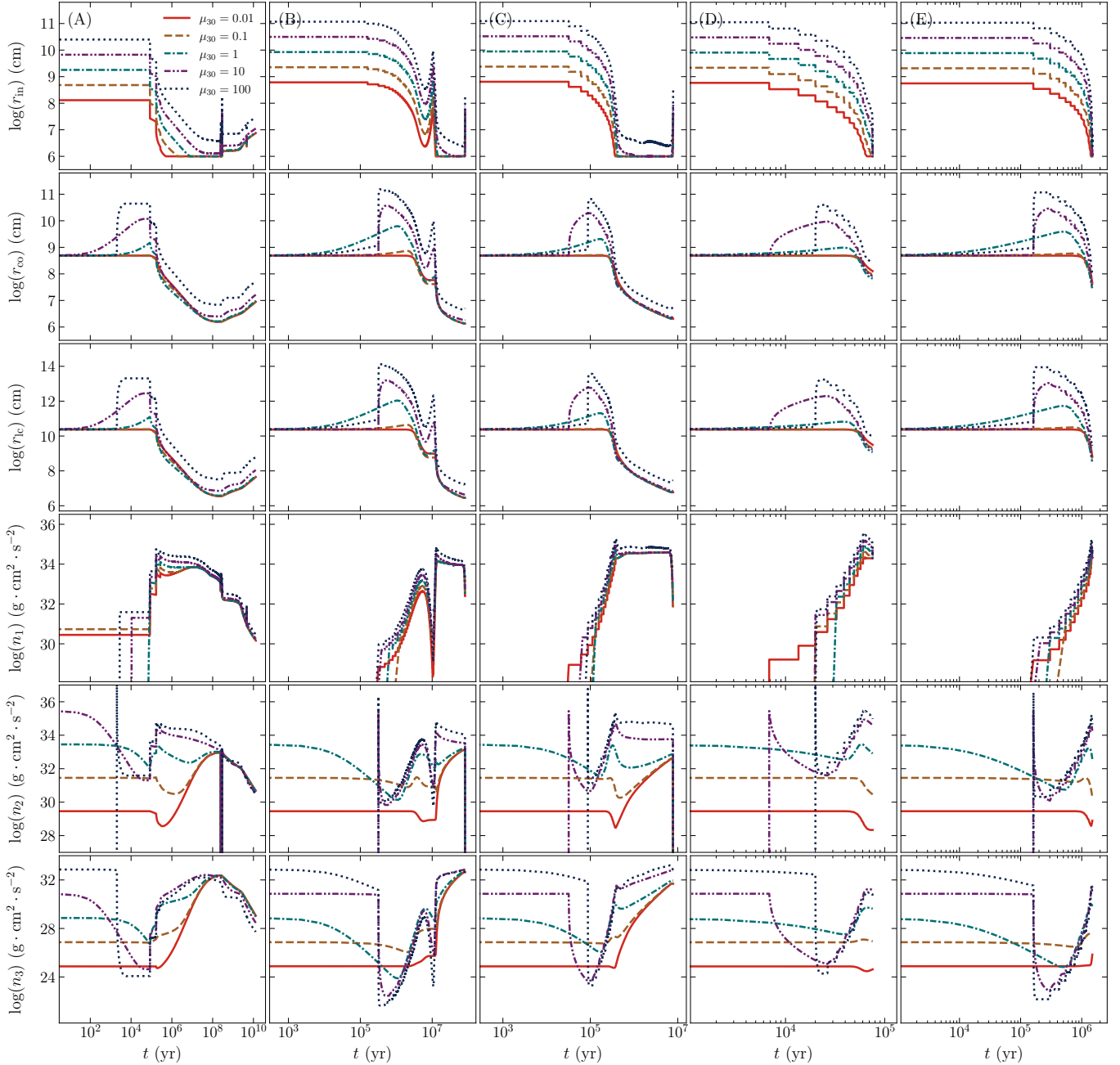


Figure 3. Evolution of the three radii and the three torques with different initial magnetic moments. The other initial parameters are $\alpha_0 = 45^\circ$, $\chi_0 = 60^\circ$, and $P_0 = 5$ s.

We then calculate the evolution for the five systems with α_0 and χ_0 randomly distributed between 0° and 180° . Figure 5 shows the variations of the magnetic inclination angles $\Delta\chi$ in the $\chi_0 - \alpha_0$ plane. Each panel corresponds to a system with a designated initial magnetic dipole moment $\mu_{30,0}$. We also depict the probability distribution of the final magnetic inclination angles χ_f with the green histogram in each panel (to be discussed below). It is apparent to see the upper and lower symmetry and mirror symmetry in left and right due to the spherical symmetry of the NS. And as mentioned above,

in most cases the magnetic axis tends to misalign with the spin axis of the NSs except for system A and for some cases in other systems with $\mu_{30,0} \geq 100$, in which the magnetic axis tends to align with the spin axis.

4. DISCUSSION

4.1. The effect of transient accretion

In last section we infer the NS accretion rate from the mass transfer rate in I/LMXBs to trace the evolution of the NS. However, it is well known that most LMXBs are transients

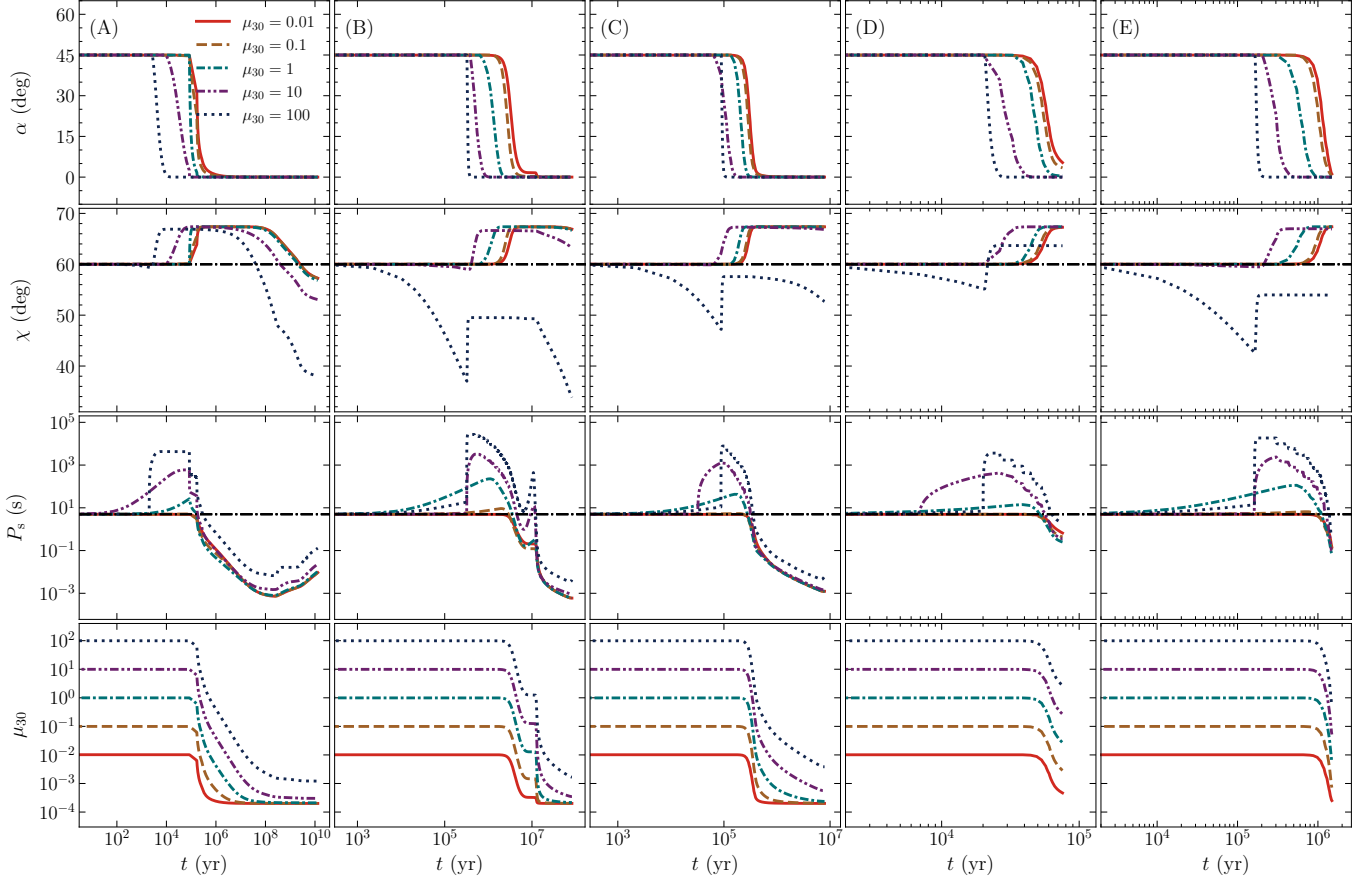


Figure 4. Same as Fig. 3, but for the evolution of the spin inclination angle α , the magnetic inclination angle χ , the spin period P_s , and the magnetic moment μ_{30} .

with rapid accretion during short outbursts separated by long quiescence. The origin of the transient behavior is likely related to the thermal and viscous instability, which occurs when the mass transfer rate \dot{M} is below a critical value (Laisa 2001),

$$\dot{M}_{\text{cr}} \simeq 3.2 \times 10^{-9} \left(\frac{M_*}{1.4 M_{\odot}} \right)^{0.5} \left(\frac{M_d}{1.0 M_{\odot}} \right)^{-0.2} \times \left(\frac{P_{\text{orb}}}{1.0 \text{ d}} \right)^{1.4} M_{\odot} \text{ yr}^{-1}. \quad (14)$$

Limit cycles of the accretion rate in the disk results in the transition from quiescence to outburst when the disk gets hot enough and hydrogen is ionized from a cooler and predominantly hydrogen neutral state. This means that a transient NS would attain a higher accretion rate during outbursts than the long-term average mass transfer rate. With that in mind, the accretion rates should be reformulated as:

$$\dot{M}_{\text{acc}} = \begin{cases} \dot{M}_{\text{di}}, & \text{if } \dot{M} \leq \dot{M}_{\text{cr}} \\ \min(\dot{M}, \dot{M}_{\text{Edd}}), & \text{if } \dot{M} > \dot{M}_{\text{cr}}, \end{cases} \quad (15)$$

where \dot{M}_{di} is the accretion rate when the disk is subject to the thermal and viscous instability. We simply assume that

the accretion rate is enhanced to $1/f$ times of \dot{M} during outbursts for a given outburst duty cycle f , and declines to zero at quiescence (see also Bhattacharyya & Chakrabarty 2017), that is

$$\dot{M}_{\text{di}} = \begin{cases} \dot{M}_{\text{burst}} = \min\left(\frac{\dot{M}}{f}, \dot{M}_{\text{Edd}}\right), & \text{during outbursts} \\ \dot{M}_{\text{qu}} = 0, & \text{during quiescence.} \end{cases} \quad (16)$$

We recalculate the evolution of the five systems with disk instability considered. The initial parameters are set to be: $\alpha_0 = 45^\circ$, $\chi_0 = 60^\circ$, $P_0 = 5 \text{ s}$, and $\mu_{30,0} = 1$. The results are compared with the reference model with the same parameters but without disk instability considered (in solid line) in Figure 6. The dashed and dot-dashed lines correspond to $f = 0.1\%$ and 1% , respectively. And the insets in the second row demonstrate the detailed evolution of α , χ and P_s when disk instability is considered.

Except for system B, which is subject to the disk instability during the whole mass transfer process, all systems generally experience the transient behavior during the early evolutionary stage when \dot{M} is low and rising (and during the late stage for system A when \dot{M} is declining). It is interesting to

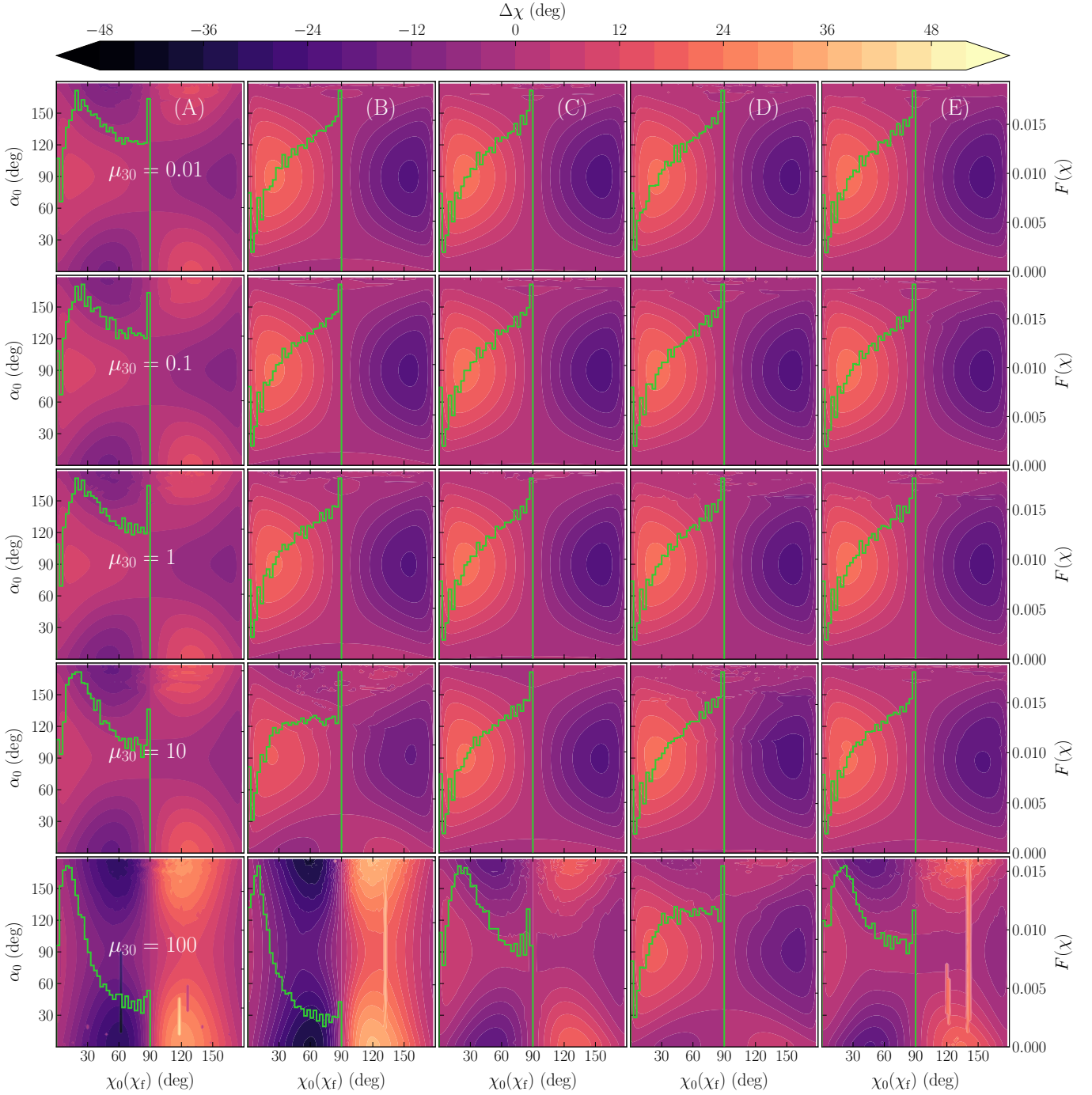


Figure 5. The variations of the magnetic inclination angles $\Delta\chi$ for the five systems with different initial magnetic moments in the $\chi_0 - \alpha_0$ plane. The green lines represent the probability distribution of the final magnetic inclination angles χ_f .

compare the magnetic inclination evolution when the mass transfer rate $\dot{M} < \dot{M}_{\text{cr}}$. In the case that disk instability is not considered, the accretion torque n_1 is relatively small or even zero (if $r_{\text{in}} > r_{\text{co}}$), so there would be little or no change in α , and χ decreases mainly due to magnetic dipole radiation according to Eqs. (2) and (3). If the disk instability is taken into account, the enhancement of the accretion rate during outbursts would exert an efficient torque on the NS, causing

both α and χ to evolve more rapidly and earlier. We can estimate the time-averaged accretion torque $\langle n_1 \rangle$ to be

$$\begin{aligned} \langle n_1 \rangle &= \dot{M}_{\text{burst}} (GM_* r_{\text{in,burst}})^{1/2} \cdot f \\ &= n_1(\dot{M}) \left(\frac{r_{\text{in,burst}}}{r_{\text{in}}} \right)^{1/2} \end{aligned} \quad (17)$$

where $r_{\text{in,burst}}$ is the inner disk radius during outbursts.

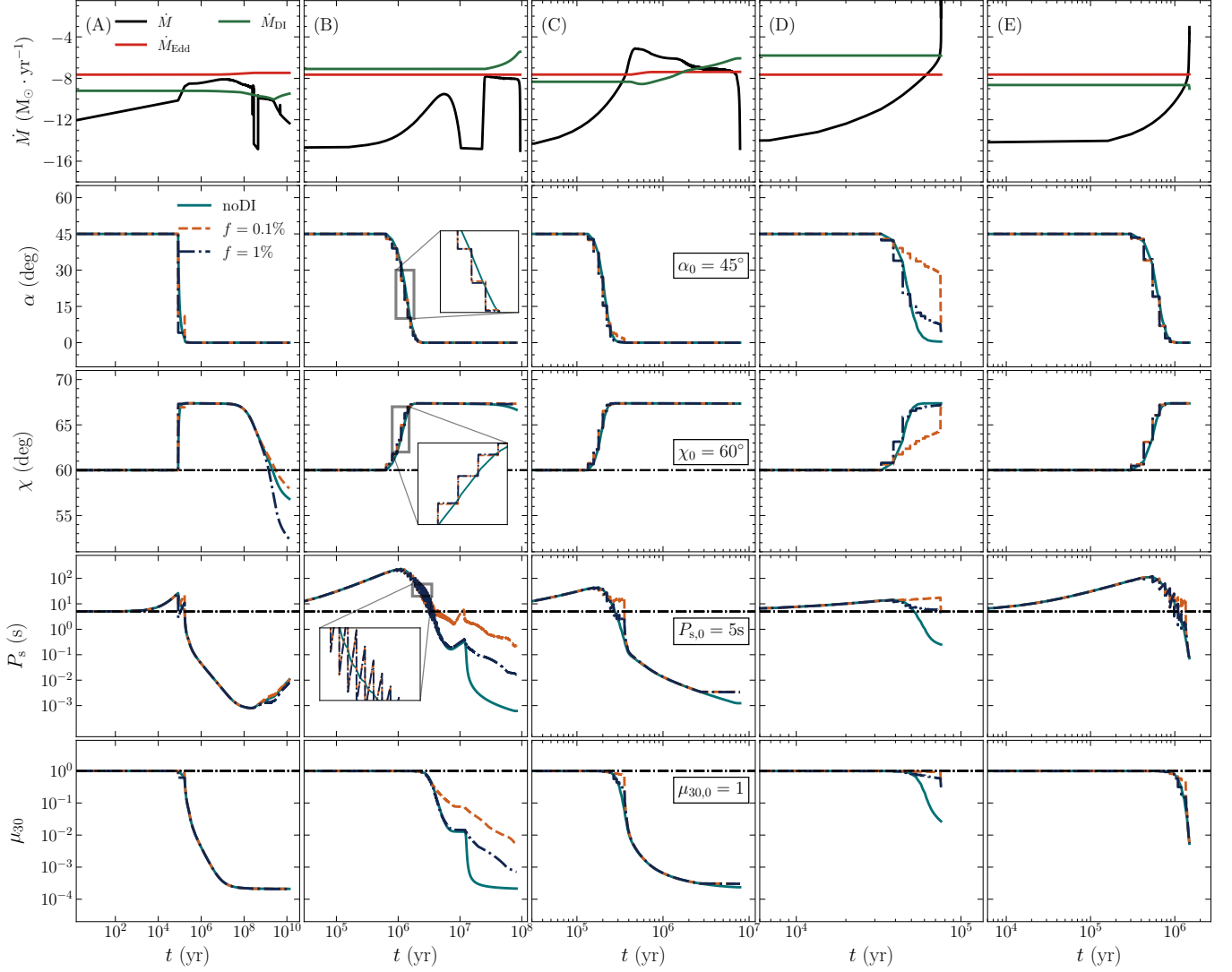


Figure 6. The solid and dashed lines compare the results in the reference model and that with the disk instability considered. The initial parameters are $\alpha_0 = 45^\circ$, $\chi_0 = 60^\circ$, $P_0 = 5\text{s}$, and $\mu_{30,0} = 1$.

For systems B-E, considering the disk instability does influence the evolutionary paths of χ , but barely affects the magnitude of χ_f . However, the disk instability has an important impact on the evolution of the spin period and the magnetic moment, especially for wide binaries such as system B, where the mass transfer rates are smaller than the criteria all the time and then $\langle n_1 \rangle$ is always $< n_1$. Consequently less material is accreted by the NS and less field decay occurs.

4.2. The effect of pulsar loss torque enhancement

Parfrey et al. (2016) proposed that the presence of a conducting disk around the NS can increase the number of open magnetic field lines and pulsar loss, in particular for rapid rotators. Under this circumstance, the torque n_3 related to

pulsar loss is amplified to be

$$n_{3,\text{parf}} = \left(\zeta \frac{r_{\text{lc}}}{r_{\text{in}}} \right)^2 n_3 \simeq -1.65 \times 10^{33} \dot{M}_2^{4/7} M_{*,\odot}^{2/7} \mu_{30}^{6/7} \Omega \text{ g cm}^2 \text{ s}^{-2}, \quad (18)$$

where ζ is used to describe the efficiency of the field line opening by the differential rotation between NS and the disk, and we take $\zeta = 1$. Therefore, the total torque exerted on the NS should be rewritten as:

$$n_{\text{tot}} = \begin{cases} n_1 + n_2 + n_{\text{parf}}, & \text{if } r_{\text{in}} < r_{\text{co}} \\ n_2 + n_{\text{parf}}, & \text{if } r_{\text{co}} \leq r_{\text{in}} < r_{\text{lc}} \\ n_3, & \text{if } r_{\text{in}} \geq r_{\text{lc}}. \end{cases} \quad (19)$$

We recalculate the evolution with the initial parameters same as in the previous section and present the results in Figure 7.

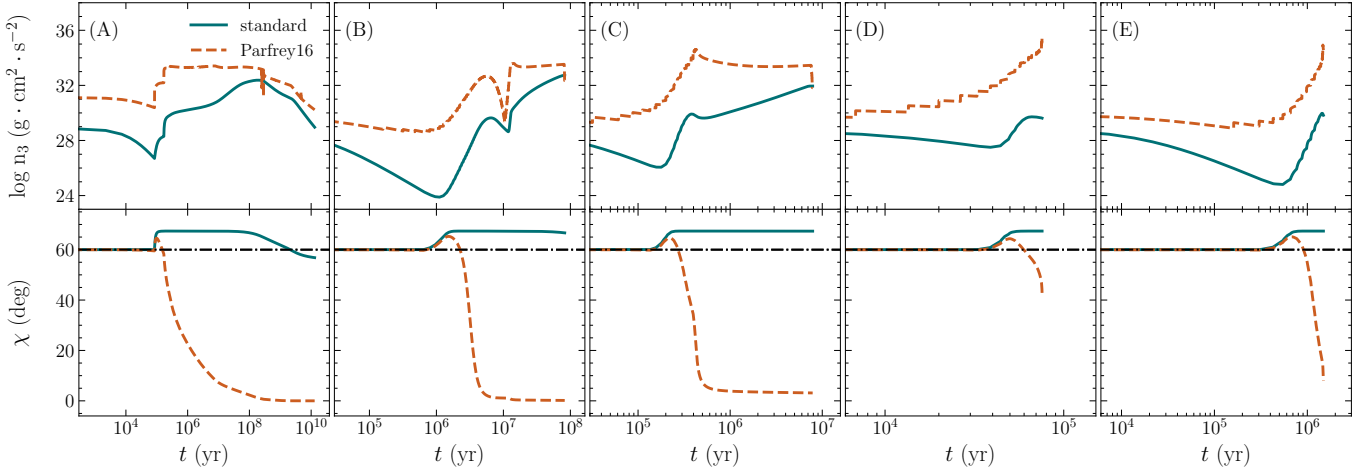


Figure 7. The solid and dashed lines compare the evolution of the magnetic inclination angles without and with torque enhancement considered. The initial parameters are same as in Figure 6.

The upper panel compares the torque n_3 and the lower panel shows its effect on the evolution of the magnetic inclination angles χ for the five systems. It is evident that the torque enhancement plays an important role in the late evolution of χ . Consequently, the magnetic axis tends to align with the spin axis, which is basically consistent with the conclusion by BA21.

4.3. Predictions of the χ distributions

Based on the above calculations, we attempt to predict the possible distributions of the magnetic inclination angles for NSs evolved from I/LMXBs. We recall that the five selected systems (A-E) correspond to different evolutionary outcomes of NS I/LMXBs, namely X-ray pulsars in UCXBs (A), BMSPs with He WD companions (B) and with CO WD companions (C), and ULXs (D and E).

In Figure 5, we depict the probability distribution functions F_χ of the final magnetic inclination angles χ_f denoted by $F_\chi = \frac{1}{N} \int n_\chi d\chi$ assuming that α_0 and χ_0 are uniformly distributed between 0° to 180° . Here $N = 8100$ is the total sample number for each type of system, and n_χ is the number of the sample with $\chi_f \in (\chi - d\chi/2, \chi + d\chi/2)$ and $d\chi = 3^\circ$. Due to the symmetry in χ_f as seen in Figure 5, we limit the abscissa range to $0^\circ - 90^\circ$ by folding the χ_f values larger than 90° .

From left to right, the first column of Figure 5 illustrates the probability distribution function for system A. It is clearly seen that the distribution of χ_f is clustered around relatively small angles (less than 30°). With increasing $\mu_{30,0}$, the χ_f 's distribution becomes more concentrated and the peak angle becomes smaller. This might partly explain why only a small amount of NS LMXBs show pulsations. The distribution functions for BMSPs evolved from systems B and C are presented in the second and third columns, respectively. They tend to possess large χ_f , roughly peaked around 90° when

$\mu_{30,0} \leq 10$. When $\mu_{30,0}$ becomes larger, the χ_f 's distribution becomes flatter because of shorter accretion time. When $\mu_{30,0} = 100$, another peak appears at $\sim 20-30^\circ$. Overall, relatively large χ_f in BMSPs are expected if $\mu_{30,0} \leq 10$, which actually favors detection of pulsations from these systems. Johnson et al. (2014) simulated the observed light curves for more than 40 MSPs detected with *Fermi*/LAT and concluded that the best-fit magnetic inclination angles are almost evenly distributed between 10° and 90° . More recently, Benli et al. (2021) selected several radio-loud millisecond gamma-ray pulsars showing double peaks in their gamma-ray profiles with the spin period P_s in the range of 2–6 ms. Their best fits suggested the magnetic inclinations χ are larger than approximately 45° . The difference in the predicted χ distributions of UCXBs and BMSPs could be useful in testing the evolutionary models and constraining the initial parameters at the NS's birth.

We use systems D and E to simulate the formation of pulsars in ULXs. The fourth and fifth columns show similar distributions of χ when $\mu_{30,0} \leq 10$, independent of the initial magnetic moment: relatively large χ s are expected for the pulsars in ULXs. When $\mu_{30,0} = 100$, the χ_f 's distribution becomes flatter in system D and peaks around 30° in system E.

We emphasize that the above results are based on the assumption that the initial spin inclination angles α and the magnetic inclination angles χ are evenly distributed between 0° and 180° . The realistic distributions must be more complicated and beyond the scope of this paper, but the general feature may not change significantly. Future observations and simulations of different types of pulsars may present more stringent constraints on their original distributions.

5. CONCLUSIONS

In this paper, we investigate the long-term magnetic inclination angle evolution of accreting NSs in I/LMXBs by combining the BA21 model with detailed binary evolution calculation. We consider five representative binary systems to reflect the formation of UCXBs, BMSPs, and ULXs. We find that the evolution of χ generally experiences at least part of the three stages: (1) during the first $10^4 - 10^5$ yr mass transfer, χ does not change much due to the relatively low mass transfer rate \dot{M} ; (2) with the growth of \dot{M} and the accretion torque, χ increases and settles at its maximum after the spin inclination angle α evolves to 0° ; (3) the pulsar loss torque drives χ to decrease. We also show that stronger initial magnetic field causes the magnetic axis to be more aligned with the spin axis for systems A, B, and C with stable mass transfer, but has little effect in systems D and E with delayed unstable mass transfer.

Moreover, considering disk instability can advance the evolution of χ , but does not significantly change the final outcome except for system A. However, the enhancement of the pulsar loss torque caused by field line opening can strongly influence the evolution of χ if it really works.

Our results suggest possible distributions of the magnetic inclination angles in specific types of binary systems including UCXBs, BMSPs and ULXs. If the initial magnetic moments of NSs are moderate, BMSPs likely have rela-

tively large magnetic inclination angles; if the NSs are initially magnetars, we expect more systems with small χ to be observed in BMSPs. Moreover, relatively small and large magnetic inclination angles are anticipated for UCXBs and ULXs, respectively.

Besides the uncertainties in both theory and observation related to the χ distribution, the main issue in this work is that the objects are limited to NSs in I/LMXBs, which are just a small portion of the NS population. Including other populations such as isolated NSs and those embedded in HMXBs will definitely provide more comprehensive understanding of the magnetic inclination evolution, and worth to be explored further.

ACKNOWLEDGMENTS

This work was supported by the National Key Research and Development Program of China (2021YFA0718500), the Natural Science Foundation of China under grant No. 12041301, 12121003, and Project U1838201 supported by NSFC and CAS.

DATA AVAILABILITY

The *MESA* code, the input files necessary to reproduce our simulations, and the associated data products are available at [zenodo.7123729](https://zenodo.org/record/7123729). The other data and codes underlying this article will be shared on reasonable request to the authors.

REFERENCES

- Annala, M. & Poutanen, J. 2010, *A&A*, 520, A76.
doi:10.1051/0004-6361/200912773
- Benli, O., Pétri, J., & Mitra, D. 2021, *A&A*, 647, A101.
doi:10.1051/0004-6361/202039853
- Bessolaz, N., Zanni, C., Ferreira, J., et al. 2008, *A&A*, 478, 155.
doi:10.1051/0004-6361/20078328
- Bhattacharya, D. & van den Heuvel, E. P. J. 1991, *PhR*, 203, 1.
doi:10.1016/0370-1573(91)90064-S
- Bhattacharyya, S. & Chakrabarty, D. 2017, *ApJ*, 835, 4.
doi:10.3847/1538-4357/835/1/4
- Biryukov, A. & Abolmasov, P. 2021, *MNRAS*, 505, 1775.
doi:10.1093/mnras/stab1378
- Bulik, T., Gondek-Rosińska, D., Santangelo, A., et al. 2003, *A&A*, 404, 1023. doi:10.1051/0004-6361:20030555
- Ghosh, P. & Lamb, F. K. 1979, *ApJ*, 234, 296. doi:10.1086/157498
- Johnson, T. J., Venter, C., Harding, A. K., et al. 2014, *ApJS*, 213, 6.
doi:10.1088/0067-0049/213/1/6
- Kulkarni, A. K. & Romanova, M. M. 2013, *MNRAS*, 433, 3048.
doi:10.1093/mnras/stt945
- Lasota, J.-P. 2001, *NewAR*, 45, 449.
doi:10.1016/S1387-6473(01)00112-9
- Leahy, D. A. 1990, *MNRAS*, 242, 188.
doi:10.1093/mnras/242.2.188
- Liu, B.-S. & Li, X.-D. 2019, *Research in Astronomy and Astrophysics*, 19, 044. doi:10.1088/1674-4527/19/3/44
- Long, M., Romanova, M. M., & Lovelace, R. V. E. 2005, *ApJ*, 634, 1214. doi:10.1086/497000
- Lyne, A. G. & Manchester, R. N. 1988, *MNRAS*, 234, 477.
doi:10.1093/mnras/234.3.477
- Parfrey, K., Spitkovsky, A., & Beloborodov, A. M. 2016, *ApJ*, 822, 33. doi:10.3847/0004-637X/822/1/33
- Paxton, B., Bildsten, L., Dotter, A., et al. 2011, *ApJS*, 192, 3.
doi:10.1088/0067-0049/192/1/3
- Paxton, B., Cantiello, M., Arras, P., et al. 2013, *ApJS*, 208, 4.
doi:10.1088/0067-0049/208/1/4
- Paxton, B., Marchant, P., Schwab, J., et al. 2015, *ApJS*, 220, 15.
doi:10.1088/0067-0049/220/1/15
- Paxton, B., Schwab, J., Bauer, E. B., et al. 2018, *ApJS*, 234, 34.
doi:10.3847/1538-4365/aaa5a8
- Paxton, B., Smolec, R., Schwab, J., et al. 2019, *ApJS*, 243, 10.
doi:10.3847/1538-4365/ab2241
- Pylyser, E. & Savonije, G. J. 1988, *A&A*, 191, 57
- Pylyser, E. H. P. & Savonije, G. J. 1989, *A&A*, 208, 52

- Rankin, J. M. 1990, *ApJ*, 352, 247. doi:10.1086/168530
- Ritter, H. 1988, *A&A*, 202, 93
- Romanova, M. M., Koldoba, A. V., Ustyugova, G. V., et al. 2021, *MNRAS*, 506, 372. doi:10.1093/mnras/stab1724
- Romanova, M. M. & Owocki, S. P. 2015, *SSRv*, 191, 339. doi:10.1007/s11214-015-0200-9
- Shibazaki, N., Murakami, T., Shaham, J., & Nomoto, K. 1989, *Nature*, 342, 656
- Venter, C., Harding, A. K., & Guillemot, L. 2009, *ApJ*, 707, 800. doi:10.1088/0004-637X/707/1/800
- Wang, Y.-M. & Welter, G. L. 1981, *A&A*, 102, 97
- Wang, Y.-M. 1987, *A&A*, 183, 257
- Young, M. D. T., Chan, L. S., Burman, R. R., et al. 2010, *MNRAS*, 402, 1317. doi:10.1111/j.1365-2966.2009.15972.x
- Zhang, C.-M. & Kojima, Y. 2006, *MNRAS*, 366, 137